Chinese Chemical Letters 37 (2026) 111203

Contents lists available at ScienceDirect

Chinese Chemical Letters

journal homepage: www.elsevier.com/locate/cclet

Multiscale "pore-film" cross-linked photothermal hygroscopic sponge for solar-driven atmospheric water harvesting

Yan Li[a], Minmin Li[a], Fan Dong[b], Wen Cui[a,c,*]

[a] College of Resources and Environmental Engineering, Key Laboratory of Karst Georesources and Environment, Guizhou University, Guiyang 550025, China
[b] Research Center for Carbon-Neutral Environmental & Energy Technology, Institute of Fundamental and Frontier Sciences, University of Electronic Science and Technology of China, Chengdu 611731, China
[c] Guizhou Karst Environmental Ecosystems Observation and Research Station, Ministry of Education, Guiyang 550025, China

ARTICLE INFO

Article history:
Received 10 March 2025
Revised 8 April 2025
Accepted 11 April 2025
Available online 12 April 2025

Keywords:
Sorption-based atmospheric water harvesting
Pore-film structure
Hygroscopic sponge
Photothermal conversion
Mass and heat transfer

ABSTRACT

Freshwater scarcity is exacerbated by uneven distribution of limited freshwater resources and high energy costs of desalination technologies. Atmospheric water vapor, a vast and geographically unrestricted reservoir, could become a sustainable alternative. Sorption-based atmospheric water harvesting (SAWH) has emerged as an available solution, yet conventional desorption methods relying on energy-intensive electrical heating hinder its scalability. Herein, a photothermal hygroscopic sponge has been developed for solar-driven atmospheric water harvesting. The composites combine a malleable melamine sponge skeleton, lithium chloride as a hygroscopic agent, and hydrangea-like molybdenum disulfide as a photothermal component, forming a multiscale "pore-film" cross-linked structure by an eco-friendly immersion-freeze-drying method. The optimized sample achieves exceptional hygroscopic capacity (3.92 g/g at 90 % RH) and freshwater production efficiency (87.77 %), which is attributed to synergistic effects of porous skeleton based crosslinked structures and "pore-film" structures, and outstanding photothermal conversion efficiency of MoS_2. The unique structure could stabilize LiCl to prevent leakage, increase mass transfer effectiveness of whole SWAH process, and enable flexibility for diverse applications. We carried out outdoor experiments to demonstrate a solar-driven water production rate of 4.22 $L\,m^{-2}\,d^{-1}$ without external energy input. This work provides insights into sustainable freshwater generation and promotes green energy utilization in addressing global water scarcity.

© 2025 Published by Elsevier B.V. on behalf of Chinese Chemical Society and Institute of Materia Medica, Chinese Academy of Medical Sciences.

Freshwater scarcity, which is exacerbated by population growth and industrialization, poses a mounting global challenge [1–4]. Existing freshwater resources (2.5 % of total water) are severely constrained and unevenly spread across the globe, which results in overabundance in some areas and significant scarcity in others [5]. Although seawater (96.5 % of all water resources [6,7]) has become one of the solutions through desalination technologies, high carbon footprints and high costs could not be ignored during the processes of reverse osmosis and multi-effect distillation [8–11]. It's noteworthy that, aside from liquid water resources, the atmosphere contains approximately 13,000 billion tons of water vapor [12–15], and importantly, it is characterized by evenly global distribution and unrestricted by the geographical location. Moreover, the atmospheric water cycle serves as the most active and crucial hub within the global water cycle, which guarantees continuous regeneration through natural processes like surface evaporation [16]. Therefore, the water vapor in atmosphere could be the potential supplier of freshwater resources, and harnessing atmospheric water for freshwater extraction has become a promising strategy to alleviate freshwater crisis.

Sorption-based atmospheric water harvesting (SAWH) is one of the most widely employed and accessible technologies, which involves the adsorption of moisture from air by sorbents, the desorption of adsorbed water by additionally heating the saturated sorbents, and the collection of liquid water through condensation [9,15,17]. Reasonable selection and design of sorbent are the primary considerations in SAWH, and the adsorption/desorption performance of water vapor directly determines the efficiency of atmospheric water collection [18]. Generally, hygroscopic salts are prevalent sorbent candidates due to their cost-effectiveness and exceptional moisture uptake capabilities across broad humidity ranges [17]. However, hygroscopic salt is easy to deliquesce after moisture uptake, which limits the reuse and thus leads to the deteriorated cyclic stability [19,20]. Meanwhile, the tendency toward aggregation of powdery hygroscopic salt could induce the slug-

* Corresponding author.
E-mail address: wcui@gzu.edu.cn (W. Cui).

https://doi.org/10.1016/j.cclet.2025.111203
1001-8417/© 2025 Published by Elsevier B.V. on behalf of Chinese Chemical Society and Institute of Materia Medica, Chinese Academy of Medical Sciences.

gish adsorption-desorption dynamics and thus decrease the mass transfer effectiveness of water vapor [21,22]. Correspondingly, recent research has gradually focused on combining hygroscopic salts with porous skeleton (MIL-101 [23,24], MOF-808 [25], hollow carbon sphere [26], activated carbon fiber [27], activated carbon cloth [28], polymer hydrogels [29,30], *etc.*), and even constructing unique pore structure of hygroscopic salt, which aims to prevent the leakage of salt solution and accelerate the mass transfer process. Representative examples include the LiCl@rGO-SA composite with directional pores for rapid kinetics [31], and dual-network hydrogels preventing salt agglomeration [32].

Apart from pursuing the effective adsorption of atmospheric water, how to realize the desorption of adsorbed water for the pure water collection is equally important. In general, traditional methods of water desorption heavily rely on electrical heating, which is not only energy-consuming but also impractical for the regions with power shortage [33,34]. This high-energy consumption and lack of accessibility pose significant challenges for sustainable water production. Therefore, developing alternative desorption technologies that are energy-efficient and universally applicable has become imperative for practical freshwater extraction. Incorporating materials with superior photothermal conversion properties into sorbents is an accessible approach to realize water desorption through solar-driven photothermal conversion effects [17,35]. For example, He *et al.* designed a carbon nanotube-based photothermal interlayer enabling efficient interfacial delamination, thereby enhancing cyclic desorption efficiency in hydrogel-based AWH systems [36]. Tan *et al.* developed a sandwich-like structure by coating photothermal Cu_xS and hygroscopic Al-Fu on both sides of a Cu sheet to realize the efficient desorption of water vapor [37]. Therefore, the integration of materials with superior photothermal conversion properties into hygroscopic material could harnesses solar energy to meet low-carbon sustainability demands while eliminating reliance on conventional electrical heating.

Herein, a hygroscopic sponge with photothermal effect has been proposed for the integration of atmospheric water sorption and solar-driven water production. Specifically, we carefully selected malleable melamine sponge (MS) as porous skeleton, typical hygroscopic salt lithium chloride (LiCl) as sorbent, nanosheets stacked hydrangea-like molybdenum disulfide (MoS_2) as photothermal material to construct a micro/millimeter-scale multilayered "pore-film" crosslinked structure by a green and straightforward immersion and freeze-drying method. The internally and externally refined structure achieved efficient and persistent hygroscopicity (3.92 g/g at 90 % RH) and outstanding production efficiency of freshwater (87.77 %), which could be attributed to the synergistic effect of the porous skeleton based crosslinked structures and "pore-film" structures, and the excellent photothermal conversion efficiency of hydrangea-like MoS_2. The crosslinked structures could stabilize the hygroscopic salt and thus prevent the leakage of salt solution, making sure subsequent water harvesting and also endowing favorable cycling stability. The micro/millimeter-scale multilayered "pore-film" structures significantly increase specific surface area and provide skillfully pathways for the transfer of water and light, accelerating the adsorption-desorption kinetics of water vapor and thus increasing mass transfer effectiveness of whole SWAH process. Besides, the porous MS could contribute to the uniform loading of LiCl and MoS_2 and provide flexibility and adaptability for various practical application scenarios. We also assessed the practical applicability of prepared sample through outdoor experiments, and the solar-driven water production rate achieved 4.22 $L\,m^{-2}\,d^{-1}$, which realizes atmospheric water harvesting without any additional energy consumption in the real environment. Therefore, this work designs a sustainable, economical, efficient and accessible solar-driven SAWH system, which offers novel insights to harness atmospheric water for alleviating freshwater scarcity and advances the development of green energy transformation and utilization.

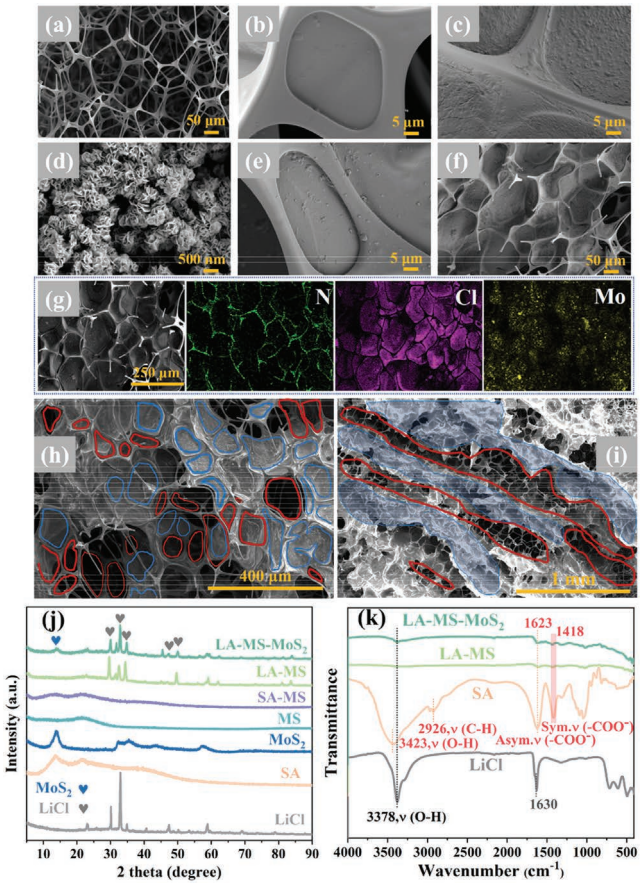


Fig. 1. The morphological structure and chemical composition of the samples. (a) MS. (b) SA-MS. (c) LA-MS. (d) MoS_2. (e) SA-MS-MoS_2. (f) LA-MS-MoS_2 surface (small scale). (h) LA-MS-MoS_2 surface (large scale). (i) Cross-section of LA-MS-MoS_2 SEM images. (g) EDS mapping spectrum of LA-MS-MoS_2. (j) XRD pattern and (k) FT-IR spectrum of prepared samples.

In this work, LA-MS-MoS_2 was synthesized through a green and straightforward immersion and freeze-drying method, and the schematic diagram of the synthesis route of LA-MS-MoS_2 is shown in (Fig. S1 (Supporting information). By using MS as a porous skeleton, SA was uniformly mixed with MoS_2 and then the SA-MoS_2 suspension was impregnated into MS. After freeze-drying, SA-MS-MoS_2 was obtained. Subsequently, LiCl solution was impregnated into SA-MS-MoS_2, and the target sample LA-MS-MoS_2 was fabricated after drying in the oven. According to the observation of scanning electron microscope (SEM), MS is a three-dimensional porous skeleton with pore sizes ranging from 10 μm to 150 μm and a skeleton diameter of 5-10 μm (Fig. 1a). After the impregnation of SA solution into the MS sponge, partial porous structure of MS was used as the framework of SA to form thin films (Fig. 1b), which could provide the place for the uniform distribution of LiCl and MoS_2 (Fig. 1e). The surface of thin film became rough after cross-linking with Li^+ (Fig. 1c). It also can be seen that the "pores" in MS are crosslinked with the LA "films" (Fig. S2a in Supporting information). Hydrangea-like MoS_2 was formed by the stacked nanosheets (Fig. 1d), and the nanosheets could further promote light absorption and enhance the photothermal conversion efficiency by making full use of the refracted and reflected sunlight. Compared with MS, some pores of LA-MS-MoS_2 were filled with the LA film and MoS_2 on it (Fig. 1f and Fig. S2b in Supporting information). According to

the EDS mapping spectrum (Fig. 1g), it was intuitively seen that Cl and Mo elements were uniformly distributed on the thin film, indicating that LiCl and MoS_2 were successfully loaded onto the LA film, which effectively addresses the agglomeration of salt in salt-based composite adsorbents. Furthermore, in the SEM images of the surface and cross-section of LA-MS-MoS_2 (Figs. 1h and i, Figs. S2c-f in Supporting information), it was clearly observed that a large number of micrometer-level "pores" and "films" further formed millimeter-level "pore" channels and "film" layer structures, respectively. Therefore, water vapor could diffuse from the surface pores to the internal adsorbent, which contributes to prevent the leakage of salt solution, enhance water storage capacity and accelerate the adsorption/desorption of water; meanwhile, the "pore-film" structure is beneficial to the refraction and reflection of sunlight for the photothermal conversion induced water production.

The crystalline structure of prepared samples has been investigated by X-ray diffraction (XRD) patterns, as shown in Fig. 1j, there are broad diffraction peaks at 13.58° and 21.66° exhibited in SA, indicating the formation of amorphous structure [38]. The characteristic diffraction peaks of MoS_2 were detected at 14.125°, 35.973°, 39.511°, 43.289°, and 58.918° (PDF #75-1539) (Fig. S3a in Supporting information), confirming the successful synthesis of MoS_2. Meanwhile, the characteristic peak of MoS_2 ($2\theta = 14.125°$) appeared in the LA-MS composite, indicating the successful incorporation of MoS_2. Also, the characteristic diffraction peaks of LiCl were observed at 30.071°, 34.861°, 50.127°, 59.569°, and 62.507° (PDF #74-1972 and PDF #73-1273) (Fig. S3b in Supporting information), confirming the successful incorporation of LiCl in LA-MS and LA-MS-MoS_2. New diffraction peaks in LA-MS-MoS_2 appeared at 31.8° and 45.45°, which can be attributed to lithium alginate formed from the reaction of SA with Li^+ (Fig. S3b). Fourier transform infrared spectroscopy (FT-IR) was employed to further investigate the physicochemical interactions among LiCl, SA, and MoS_2 and the changes in chemical bonds when various monomers introduced (Fig. S4 in Supporting information). As shown in Fig. 1k, the IR peak appearing around 3378 cm^{-1} in all monomers could be attributed to the O-H stretching vibration of adsorbed water molecules [39]. In the IR spectrum of MoS_2, the peaks located at 880 and 593 cm^{-1} correspond to the S-S and Mo-S bond vibrations, respectively [40]. There are no IR peaks of MoS_2 observed in LA-MS-MoS_2, which is due to the low content of MoS_2 and partial encapsulation by SA, and it also corresponds with the SEM observations. The distinct absorption peaks of SA were observed at 2926, 1623, 1418, and 1045 cm^{-1}, corresponding to the stretching vibrations of C-H, the asymmetric and symmetric stretching vibrations of -COO-, and the stretching vibrations of C-O-C/C-O, respectively [41]. It is worth noting that the IR peak at 1418 cm^{-1} in SA changed into 1433 cm^{-1} after the impregnation with LiCl solution, reflecting the interaction between LiCl and SA by the ion exchange of Li^+ and Na^+ ions at the -COO- sites [41]. Additionally, the IR peak intensity of 1623, 1418 cm^{-1} in LA-MS-MoS_2 decreased, suggesting a strong ionic bond between Li and the alginate chains, which contributed to the secure attachment of LiCl and prevented the leakage of salt solution upon sample hydration.

In order to investigate the hydrophilic and hydrophobic properties of prepared samples, water contact angle tests were conducted on MS, SA-MS, and LA-MS-MoS_2 (Fig. 2a). It was observed that pure MS shows a contact angle of 109.97°, exhibiting hydrophobicity; the contact angle of SA-MS is 70.5°, and the sample gradually became hydrophilic along with the addition of hydrophilic SA; noteworthily, after the addition of the hygroscopic salt LiCl, water molecules were instantaneously absorbed on the sample surface within 20 ms, which reflects the superhydrophilicity of LA-MS-MoS_2. Subsequently, the optimal concentration of the hygroscopic salt LiCl in LA-MS was further explored (Fig. 2b and Fig. S5), and the moisture uptake of the sample increased significantly with the increase of LiCl concentration (0–2.5 mol/L), reaching up to 4.03, 3.55, 2.37, 1.64 g/g at 90%, 80%, 60% and 30%–40% RH, respectively. However, the overadditive LiCl (>2.5 mol/L) in the composite adsorbent could block the internal pores of sponge and thus induce the moisture uptake to stop increasing or even decrease. Therefore, 2.5 mol/L LiCl was determined to be the optimal concentration for preparing the samples, and the optimal sample (LA-MS loaded with 2.5 mol/L LiCl) still maintained good moisture uptake after five cycles (Fig. 2c). Meanwhile, we designed control experiments to further verify the excellent persistent hygroscopic property of LA-MS loaded with 2.5 mol/L LiCl, and equivalent LiCl powder and LiCl-MS that LiCl were directly impregnated onto MS have been prepared as control sample. As shown in Figs. 2d and e, it can be seen that the moisture uptake rate of LA-MS (1.50 $g\,g^{-1}\,h^{-1}$) within 1 h was 1.73 and 1.32 times that of LiCl (0.87 $g\,g^{-1}\,h^{-1}$) and LiCl-MS (1.14 $g\,g^{-1}\,h^{-1}$), respectively. Moreover, along with the hygroscopic reaction proceeds, pure LiCl completely deliquesced into salt solution within 2 h, and LiCl-MS also began to leak salt solution after 8 h. In contrast, as shown in the inset of Fig. 2d, LA-MS remained stable without any leakage after 12 h of hygroscopic reaction, which could be attributed to the unique micro/millimeter-level multilayered "pore-film" cross-linked structure. Furthermore, as shown in Fig. 2f, our synthesized samples exhibited superior performance of water vapor adsorption compared with materials in previously published works [19,32,39,42–44].

Subsequently, the promotion mechanism of hygroscopic performance has been further explored. As shown in Fig. 2g, the water vapor sorption isotherms of LA-MS-MoS_2 at 25 °C are consistent with those of salt-based composite sorbents reported in previous studies [31,41], which shows physical adsorption from 0 to 11% RH, deliquescence of the salt around 30% RH, and finally absorption by the salt solution. Furthermore, we directly observed the *in situ* hygroscopic process of LA-MS-MoS_2 by optical microscope (Fig. 2h). Initially, the water vapor diffused from the high-humidity air to the surface of the composite adsorbent; and then the surface gradually became moist and chemical adsorption occurred due to the introduced hygroscopic salt LiCl; the increasing amount of moisture gradually turned into salt solution, which was gathered and stored on the "films". Additionally, water molecules passed through the pore channels into the internal layers and thus water adsorption was also taken place orderly, and the hygroscopic process was similar to the surface structure. Therefore, micro/millimeter-scale "pores" could act as transport channels of water vapor, providing a convenient path to the internal of adsorbent, which reduces mass transfer resistance in comparison with solid or single-pore-sized adsorbents. Moreover, the porous structure provided more internal surface area to increase the contact between water vapor and the adsorbent, thereby significantly improving the diffusion and mass transfer rate of water vapor. On the other hand, the micro/millimeter-scale "films" contributes to the uniform distribution of hygroscopic salt LiCl, which promotes the convergence and storage of moisture on the "films", and thus solving the problem of salt solution leakage. The unique "pore-film" structure not only increase the adsorption quantity of water but also enhance water storage capacity, realizing the efficient and persistent atmosphere water adsorption. The schematic diagram of atmosphere water adsorption on LA-MS-MoS_2 is illustrated in Fig. 2i.

Water desorption is another key step in SAWH, which determines the cyclic reuse of the sample and the final yield of freshwater. In order to conform the low-carbon, low-cost, and sustainable requirements, hydrangea-like MoS_2 with superior photothermal conversion properties has been integrated into hygroscopic material for the solar-driven water desorption. As shown in Fig. 3a, in comparison with LA-MS without the addition of photothermal

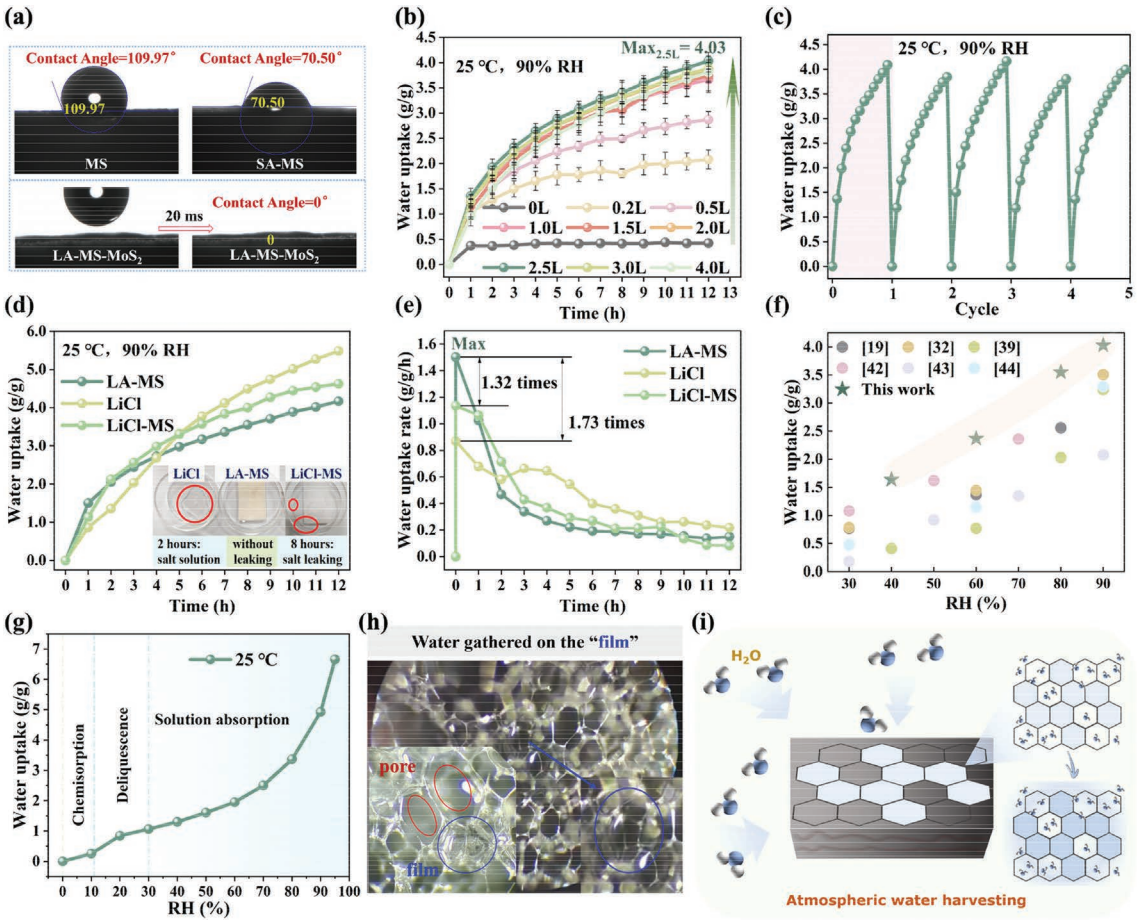


Fig. 2. Performance of water vapor adsorption of the prepared samples. (a) The contact angle of the samples. (b) The water vapor sorption kinetics of LA-MS loaded with different LiCl concentrations (0–4.0 mol/L) at 25 °C, 90 % RH. (c) The moisture adsorption cycling test of LA-MS (loaded with 2.5 mol/L LiCl) at 25 °C, 90 % RH. (d) The moisture adsorption performance test of LiCl powder (abbreviated as LiCl), LiCl solution directly impregnated onto MS samples (abbreviated as LiCl-MS), and LA-MS at 25 °C, 90 % RH, with the inset showing the corresponding moisture adsorption process and whether the salt solution leaked. (e) A comparison of the moisture adsorption rates of the samples in (d). (f) Moisture adsorption performance comparison of LA-MS with reported studies. (g) The water sorption isotherms of LA-MS-MoS_2 at 25 °C. (h) The optical microscope image of LA-MS-MoS_2 during moisture adsorption and (i) Schematic of water vapor transport from ambient air to sorbents. light blue: LA "film", dark blue: water vaper adsorbed and aggregated on the LA "film".

material, LA-MS-MoS_2 exhibits strong light absorption capabilities in the range of 280-2500 nm and achieves 94.7 % solar light absorption. Under the simulation of 1 sun (1 sun ≈ 100 mW/cm^2) irradiation (Fig. 3b), the surface temperatures of LA-MS and LA-MS-MoS_2 maintains the same variation trend, rapidly increasing within the first 15 min. Notably, the temperature of LA-MS is stable at 35 °C while LA-MS-MoS_2 keeps the surface temperature around 45 °C, along with the irradiation time increased, the adsorbed water in the sample was evaporated and then the surface temperature of LA-MS-MoS_2 continued to rise to 57.2 °C (Fig. 3c). Therefore, the hydrangea-like MoS_2 endowed the sample with excellent photothermal conversion performance to provide sufficient heat for the desorption of adsorbed water. The excellent photothermal conversion could be attributed to the unique micro and macro structure of LA-MS-MoS_2. To be specific, the nanosheets stacked hydrangea-like structure of MoS_2 is beneficial to the absorption, refraction and reflection of light, making full use of the light source. Furthermore, the pore structure could not only provide a larger surface area to allow more light energy to be absorbed, but also induce the sunlight to enter and then increase the propagation path of light to enable multiple reflections and scattering of light energy and thus improve light absorption efficiency. Additionally, LA-MS-MoS_2 also exhibited excellent thermal stability. According to thermogravimetric curve analysis (Fig. S6), the temperature of water desorption is below the decomposition temperature of the composite adsorbent, ensuring its structural stability for the regeneration and repeated use.

At the same time, we further investigated the impact of different additive amount of MoS_2 on the water desorption in the prepared SAWH system. As shown in Fig. 3d, the LA-MS-0.07MoS_2 sample shows the highest moisture uptake of 3.92 g/g after moisture adsorption for 12 h at 25 °C and 90 % RH, and simulated 1 sun irradiation was used to desorb the adsorbed water from the samples. The desorption rate of LA-MS-0.07MoS_2 is as high as 1.40 g g^{-1} h^{-1} (Fig. 3e) after 1 h of illumination, the collection amount of water is 2.91 g/g after 3 h (Fig. 3f), and the collection efficiency of water is 87.77 % (Fig. 3g). In summary, the fabricated porous structure and outstanding photothermal conversion properties of hydrangea-like MoS_2 enabled the composite adsorbent to fully absorb solar energy and convert it into thermal energy, which facilitates the desorption of water from the composite adsorbent and thereby generates freshwater, and the process of solar-driven water production was showed in Fig. 3h.

In order to further assess the practical applicability of LA-MS-MoS_2, we carried out large-scale outdoor experiments to explore the performance of LA-MS-MoS_2 for atmospheric water adsorption and solar-driven water production. As shown in Fig. 4a, twelve pieces LA-MS-MoS_2 were placed in a homemade water collection

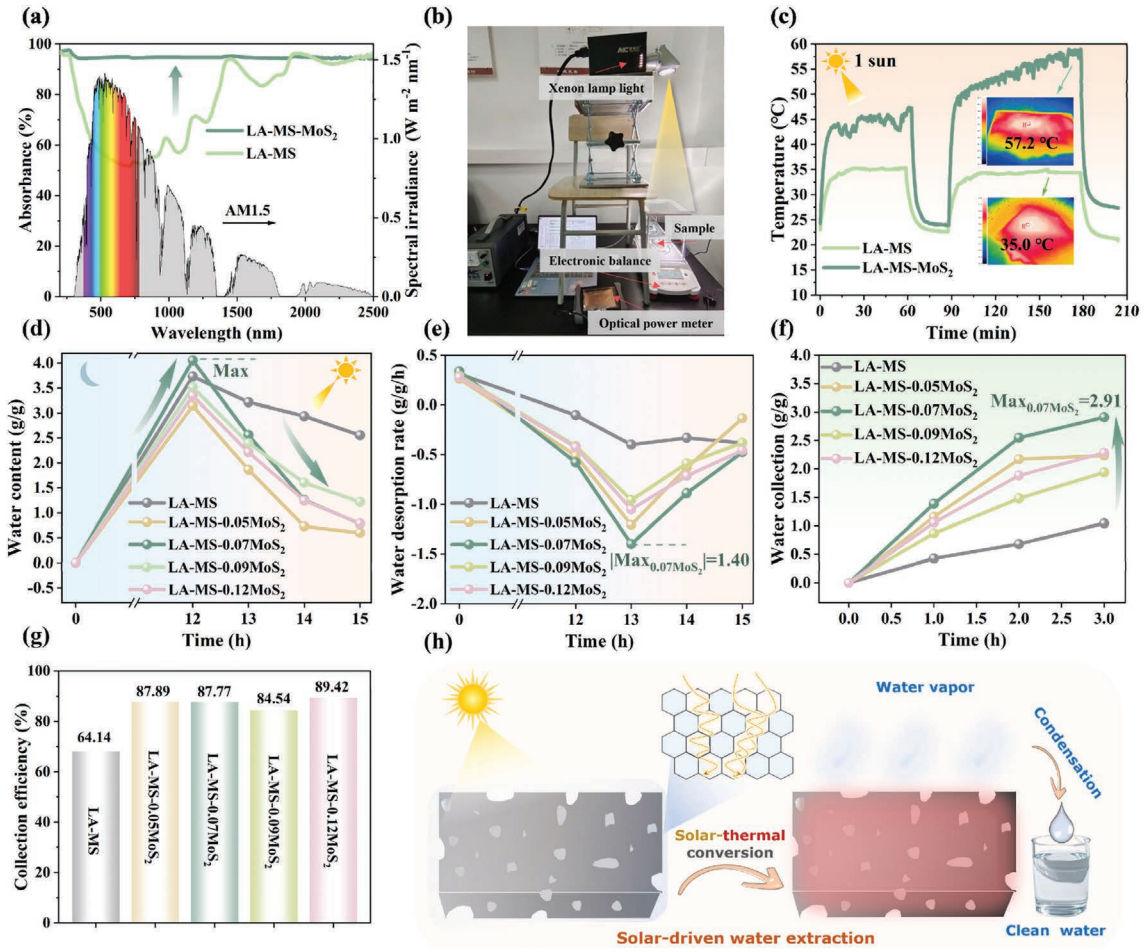


Fig. 3. Performance of solar-driven water production the prepared samples. (a) The solar light absorbance of LA-MS and LA-MS-MoS_2. (b) The device for simulated solar-driven water desorption. (c) The surface temperature changes of LA-MS and LA-MS-MoS_2 under simulated 1 sun irradiation, with samples containing different amounts of MoS_2. (d) Water adsorption desorption curves. (e) Water desorption rates. (f) Amount of water collected. The data presented above are the mean values from three experiments. (g) Effective water collection efficiency and (h) Schematic diagram of solar-driven water production.

device (Fig. S7 in Supporting information) for outdoor atmospheric water adsorption overnight (12 h), and the thermometer and hygrometer were used to record the ambient conditions in real-time (average temperature of 12 °C and average humidity of 90 % RH). The water collection device was covered with a homemade condensation lid in the following daytime, and natural sunlight was used to desorb the adsorbed water from the samples by photothermal conversion effect. During 3 h of natural sunlight exposure, a photometer was used to measure the solar power density, which ranged from 0.5 sun to 0.9 sun, and the average solar power density was 0.8 sun in the whole process of solar driven water production. It could be observed that the condensation appeared on the walls of the condensation lid within 5 min under the sunlight, and the adsorbed moisture was gradually released from the sample. As shown in Fig. 4b, the experimental device was covered with small water droplets after 180 min, and it was approximately 12 mL of water released from the samples. Due to residual moisture on the walls and heat loss, a final collection volume of 9.5 mL was obtained (Fig. 4c). The solar-driven water production rate was 4.22 L m^{-2} d^{-1}, which meets the World Health Organization's (WHO) recommended total water intake (2.9 L/d for males and 2.2 L/d for females), achieving solar-driven atmospheric water harvesting without additional energy consumption. Moreover, we carried out six outdoor tests to further demonstrate the excellent cyclic stability of LA-MS-MoS_2 (Fig. 4c and Fig. S8 in Supporting information supplemented the complete data of environmental condition, including temperature, humidity and solar radiation). The ion concentrations in the collected water were tested and the results showed that the concentrations of K^+, Ca^{2+}, Na^+, Mg^{2+}, Cl^-, F^-, NO_3^- and SO_4^{2-} ions were well below the WHO drinking water standards (Fig. 4d) [45], indicating that the collected water was safe and clean. Therefore, the multi-layered "pore-film" structured LA-MS-MoS_2 could be the candidate for the solar-driven atmospheric water collection in real environments to alleviate the shortage of freshwater resources.

In summary, this work presents a solar-driven SAWH system using a photothermal hygroscopic sponge by integrating melamine sponge, LiCl, and hydrangea-like MoS_2. The designed micro/millimeter-scale "pore-film" structure, fabricated *via* a green immersion-freeze-drying method, achieves high hygroscopicity (3.92 g/g at 90 % RH) and freshwater production efficiency (87.77 %), which is attributed to the synergistic effect of rapid adsorption-desorption kinetics, photothermal conversion, and salt stabilization to prevent leakage. Outdoor experiments also demonstrate a water yield of 4.22 L m^{-2} d^{-1} without external energy, offering a sustainable, low-cost solution to freshwater scarcity through renewable solar-driven atmospheric water utilization. This study not only contributes to the development of green water harvesting technologies but also underscores the viability of integrating renewable energy systems to address pressing environmental challenges.

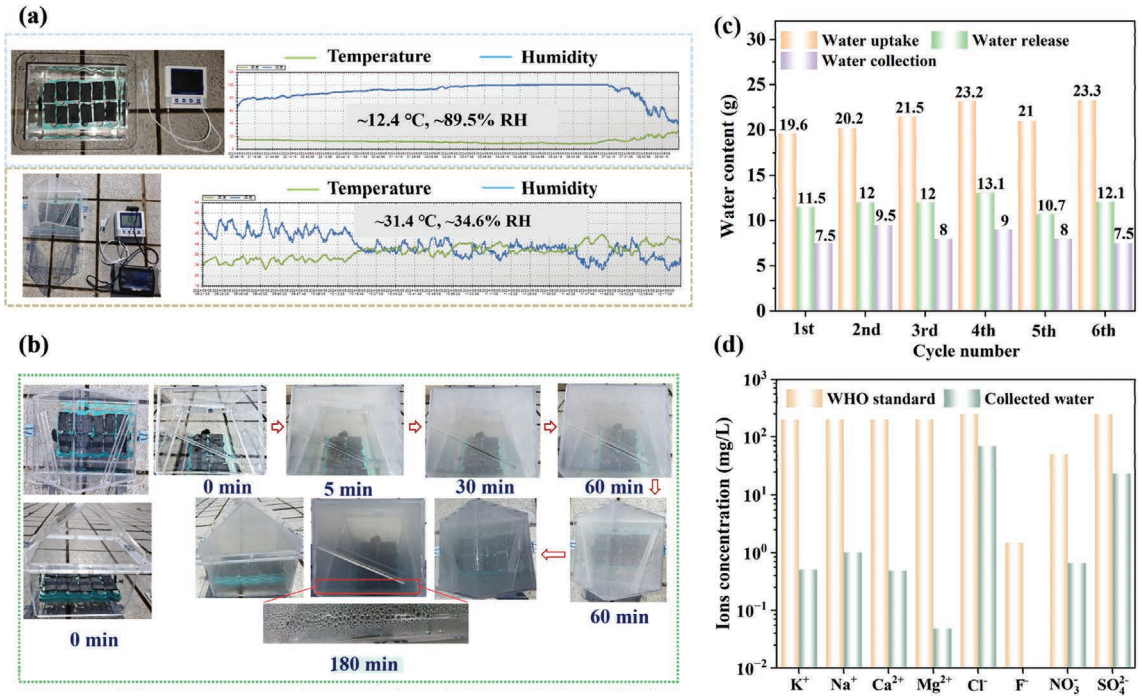


Fig. 4. Solar-driven atmospheric water harvesting outdoor experiments. (a) Twelve pieces of LA-MS-MoS_2 underwent atmospheric water adsorption for 12 h overnight (top) and water production through sunlight exposure for 3 h the following day (bottom), along with temperature and humidity changes. (b) A physical photo of solar-driven atmospheric water the next day. (c) Water uptake, water release, and water collection in six cyclic tests. (d) Water quality analysis.

Declaration of competing interest

The authors declare that they have no known competing financial interests or personal relationships that could have appeared to influence the work reported in this paper.

CRediT authorship contribution statement

Yan Li: Writing – review & editing, Writing – original draft, Methodology, Investigation, Conceptualization. **Minmin Li:** Software, Methodology, Investigation. **Fan Dong:** Writing – review & editing. **Wen Cui:** Writing – review & editing, Validation, Supervision, Project administration, Funding acquisition.

Acknowledgments

This work was supported by the National Key Research and Development Program of China (No. 2022YFC3702800), the National Natural Science Foundation of China (Nos. 22366008, 22406032), the Guizhou Provincial Basic Research Program (Natural Science) (No. ZK (2023)045).

Supplementary materials

Supplementary material associated with this article can be found, in the online version, at doi:10.1016/j.cclet.2025.111203.

References

[1] M. Peydayesh, R. Mezzenga, Chem. Soc. Rev. 53 (2024) 4333–4348.
[2] W. Mandal, S. Fajal, A.V. Desai, S.K. Ghosh, Coord. Chem. Rev. 524 (2025) 216326.
[3] Z.Y. Wang, Y.J. Zhu, Y.Q. Chen, et al., Sep. Purif. Technol. 362 (2025) 131816.
[4] R. Wang, W. He, Commun. Mater. 5 (2024) 203.
[5] G.K. Nürnberg, Lake Functioning: Internal Phosphorus Loading, Cyanobacteria, and Climate Change, CRC Press, 2024.
[6] A. Richts, W.F. Struckmeier, M. Zaepke, WHYMAP and the groundwater resources map of the world 1:25,000,000, in: J. Jones (Ed.), Sustaining Groundwater Resources. International Year of Planet Earth, Springer, Dordrecht, 2011, pp. 159–173.
[7] S.S. Veroneau, D.G. Nocera, Proc. Natl. Acad. Sci. U. S. A. 118 (2021) e2024855118.
[8] L. Wang, X. Sun, F. Gao, et al., Desalination 592 (2024) 118124.
[9] C. Lei, W. Guan, Y. Zhao, G. Yu, Chem. Soc. Rev. 53 (2024) 7328–7362.
[10] A. Rani, S.Y. Pan, S. Negi, Y. Lin, Water Res. 257 (2024) 121720.
[11] A. Naminezhad, M. Mehregan, Renew. Energy 185 (2022) 888–903.
[12] M. Ehtisham, A.K. Badawi, A.M. Khan, et al., RSC Adv. 14 (2024) 6165–6177.
[13] R.Y. Li, Y. Shi, M.C. Wu, et al., Nano Energy 67 (2020) 104255.
[14] H. Zhou, L. Yan, D. Tang, et al., Adv. Mater. 36 (2024) 2403876.
[15] C. Zeng, A. Mojiri, J. Ananpattarachai, et al., Water Res. 265 (2024) 122227.
[16] G. Zhao, Y. Li, L.M. Zhou, H.L. Gao, Nat. Commun. 13 (2022) 3686.
[17] A. Entezari, O.C. Esan, X. Yan, et al., Adv. Mater. 35 (2023) 2210957.
[18] S.X. Bai, X.X. Yao, M.Y. Wong, et al., ACS Nano 18 (2024) 31597–31631.
[19] M. Xia, D. Cai, J.B. Feng, et al., Adv. Funct. Mater. 33 (2023) 2214813.
[20] M.L. Wang, E.K. Liu, T. Jin, et al., Water Res. 250 (2024) 121052.
[21] L.Z. Ren, J.G. Cao, S.W. Liu, et al., Adv. Mater. 36 (2024) 2404758.
[22] A. Karmakar, V. Prabakaran, D. Zhao, K.J. Chua, Appl. Energy 269 (2020) 115070.
[23] J. Xu, T. Li, J. Chao, et al., Angew. Chem. Int. Ed. 59 (2020) 5202–5210.
[24] B.Q. Tan, Y.S. Luo, X.H. Liang, et al., Micropor. Mesopor. Mat. 286 (2019) 141–148.
[25] H. An, Y. Chen, Y. Wang, et al., Chem. Eng. J. 461 (2023) 141955.
[26] T. Liu, L.Y. Zhang, B. Cheng, J.G. Yu, Adv. Energy Mater. 9 (2019) 1803900.
[27] J.Y. Liu, J.Y. Wang, L.W. Wang, R.Z. Wang, Int. J. Refrig. 83 (2017) 51–59.
[28] Y.J. Duan, Y.F. Gao, Z.T. Ren, et al., Appl. Surf. Sci. 660 (2024) 159884.
[29] S. Aleid, M.C. Wu, R.Y. Li, et al., ACS Mater. Lett. 4 (2022) 511–520.
[30] H.Y. Lu, W. Shi, J.H. Zhang, et al., Adv. Mater. 34 (2022) 2205344.
[31] J.X. Xu, T.X. Li, T.S. Yan, et al., Energy Environ. Sci. 14 (2021) 5979–5994.
[32] M.Y. Song, T.S. Cheng, Y.F. Li, et al., J. Clean Prod. 461 (2024) 142661.
[33] W.W. Wang, S.T. Xie, Q.W. Pan, et al., Renew. Sustan. Energy Rev. 141 (2021) 110802.
[34] J. Canivet, A. Fateeva, Y.M. Guo, et al., Chem. Soc. Rev. 43 (2014) 5594–5617.
[35] W. Chen, Y. Liu, B. Xu, et al., Adv. Funct. Mater. 34 (2024) 2410999.
[36] Y. He, Y. Zhang, B. Xiang, et al., Adv. Funct. Mater. (2024) 2416875.
[37] Y.X. Tan, W.C. Chen, Y.T. Fang, S.F. Wang, Chem. Eng. J. 475 (2023) 146353.
[38] J. Jiang, Y. Chen, W. Wang, et al., Carbohydr. Polym. 151 (2016) 600–605.
[39] X.P. Zhang, H. Qu, X.Y. Li, et al., Adv. Mater. 36 (2024) 2310219.
[40] J. Dai, C. Yang, Y. Xu, et al., Adv. Mater. 35 (2023) 2303732.
[41] R. Zhu, Q.F. Yu, M. Li, et al., Nano Energy 124 (2024) 109471.
[42] J.J. Sun, F. Ni, J.C. Gu, et al., Adv. Mater. 36 (2024) 2314175.
[43] M.J. Li, L. Shu, X.F. Zhang, et al., Chem. Eng. J. 499 (2024) 155932.
[44] N. Ding, B. Liang, X.P. Gao, et al., Chem. Eng. J. 495 (2024) 153470.
[45] O. World HealthGuidelines For Drinking-Water Quality, 4th ed., World Health Organization, Geneva, 2011.